Journal of Materials Chemistry C

PAPER

View Article Online
View Journal

Published on 01 December 2017. Downloaded by University Town Library of Shenzhen on 02/02/2018 01:34:05.

Check for updates

Cite this: DOI: 10.1039/c7tc05063a

A chrysene-based liquid crystalline semiconductor for organic thin-film transistors†‡

Yaowu He,[a] Wenjun Xu,[a] Imran Murtaza,[bc] Chao Yao,[a] Yanan Zhu,[a] Aiyuan Li,[a] Chao He[a] and Hong Meng *[a]

Received 7th November 2017,
Accepted 1st December 2017

DOI: 10.1039/c7tc05063a

rsc.li/materials-c

We report the synthesis and characterization of a non-liquid crystalline material, 2-phenylchrysene (Ph-CHR), and a liquid crystalline material, 2-(4-dodecyl phenyl)chrysene (C12-Ph-CHR), and discuss their organic thin-film transistor (OTFT) device performances. The concept of designing chrysene derivatives is derived from the similar electronic structure of chrysene and [1]benzothieno[3,2-*b*][1]benzothiophene (BTBT), which is a very famous core for organic semiconductors. OTFTs, based on Ph-CHR and C12-Ph-CHR, are fabricated by vacuum-deposition on octyltrichlorosilane (OTS(8)) treated Si/SiO_2 substrates. Our experimental results show that OTFTs based on Ph-CHR possess higher mobility than OTFTs based on BTBT derivative 2-phenyl[1]benzothieno[3,2-*b*][1]benzothiophene (Ph-BTBT). The liquid crystalline material C12-Ph-CHR achieves the highest carrier mobility of up to 3.07 $cm^2\ V^{-1}\ s^{-1}$ with an on/off ratio of 3.3×10^6 for polycrystalline organic thin-film transistors in ambient air. The results indicate that the chrysene derivative C12-Ph-CHR is a promising candidate for applications in electronic devices.

Introduction

Organic thin film transistors (OTFTs) which have the advantages of low manufacturing costs and large area fabrication process are expected to be used as the key elements for realizing the next-generation electronics, such as for flexible displays and printed electronics.[1,2] The design and synthesis of small molecule organic materials used as semiconductors in OTFTs have increased significantly in recent years because they can be easily synthesized in large quantities and have reliable device performance. Numerous efforts regarding synthesis have been devoted to developing superior organic semiconductor materials with high charge carrier mobilities. [1]Benzothieno[3,2-*b*]-[1]benzothiophene (BTBT) derivatives have attracted scientists' attention due to their high carrier mobility and stability in ambient air. Recently, the liquid-crystalline materials based on OTFTs have attracted much interest because liquid crystals can form well-ordered polycrystalline thin-films depending on the deposition method and thermal annealing of the liquid crystal phase.[3–11] Lino and co-workers reported a liquid crystalline material Ph-BTBT-10 with Sm E phase[4] which was able to form a uniform and molecularly smooth polycrystalline thin film by using Sm E precursor thin films and achieved the highest mobility up to 13.9 $cm^2\ V^{-1}\ s^{-1}$ in OTFTs. Our group has also recently reported a series of air-stable liquid crystalline semiconductor materials based on [1]benzothieno[3,2-*b*]benzothiophene (BTBT) derivatives, which exhibit a highly ordered liquid crystal phase with high mobility in OTFTs.[12–14] However, it is still a great challenge to develop novel organic semiconductors with high mobility as well as good air stability and simple synthesis method for practical applications in OTFTs.

The structure of chrysene is composed of four aromatic rings fused in a linear manner and is similar to that of BTBT. In contrast, the synthesis method of chrysene derivatives is simpler as compared to that of the BTBT derivatives. The energy levels of BTBT, and the chrysene core were modeled by B3LYP-G*. The chemical structures, and lowest unoccupied molecular orbital (LUMO) and highest occupied molecular orbital (HOMO) levels of these two compounds are shown in Fig. 1 and the LUMO and HOMO energy levels and HOMO–LUMO gaps are summarized in Table S1 (ESI†). It can be seen that the band gaps and the HOMO energy levels of BTBT and chrysene are strikingly similar. The calculated results indicate that the chrysene and BTBT cores possess a similar electronic structure.

The charge transfer integrals were calculated from single crystals of BTBT and chrysene by modeling software.[15–17]

[a] School of Advanced Materials, Peking University Shenzhen Graduate School, Shenzhen, 518055, China. E-mail: menghong@pkusz.edu.cn
[b] Key Laboratory of Flexible Electronics (KLOFE) & Institute of Advanced Materials (IAM), Jiangsu National Synergetic Innovation Center for Advanced Materials (SICAM), Nanjing Tech University (Nanjing Tech), 30 South Puzhu Road, Nanjing 211816, China
[c] Department of Physics, International Islamic University, Islamabad 44000, Pakistan

† Celebrating 50 years of Professor Fred Wudl's contributions to Organic Electronics.

‡ Electronic supplementary information (ESI) available. See DOI: 10.1039/c7tc05063a

Published on 01 December 2017. Downloaded by University Town Library of Shenzhen on 02/02/2018 01:34:05.

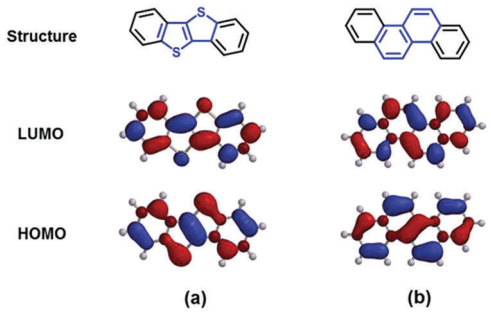

Fig. 1 The calculated frontier orbital (HOMO and LUMO) distribution of BTBT and chrysene.

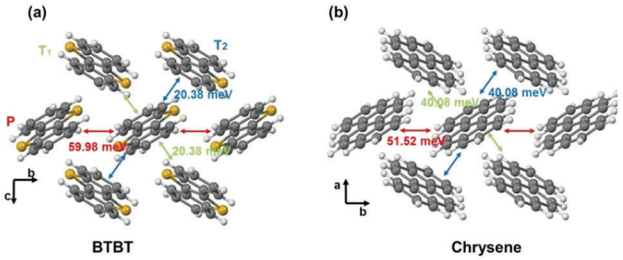

Fig. 2 Hole transfer integrals for the molecular pairs taken from single crystals of BTBT and chrysene.

As shown in Fig. 2 and Table S2 (ESI‡), chrysene exhibits strong transfer integrals of 51.52, 40.08 and 40.08 meV for all three pairs while for BTBT, strong electronic coupling is found only in one pair each. The calculation results indicate that chrysene is expected to have higher mobility than BTBT, owing to the stronger electronic couplings.

With these results and expectations in mind, we focused our attention on chrysene derivatives and successfully designed and synthesized a non-liquid crystalline material of 2-phenyl chrysene (Ph-CHR) and a liquid crystalline material of 2-(4-dodecyl phenyl) chrysene (C12-Ph-CHR). The alkyl chain can improve the carrier mobility of the materials, while the phenyl group can enhance the thermal stability and molecular density.[18] We present here an efficient synthetic method of chrysene derivatives Ph-CHR and C12-Ph-CHR, along with their electrochemical and optical properties, thin film morphology and OTFT performance. The Ph-CHR-based OTFTs show better charge transport properties than those based on BTBT derivative, Ph-BTBT.[14] OTFTs based on C12-Ph-CHR demonstrated a high carrier mobility of up to 3.07 $cm^2 V^{-1} s^{-1}$ with an on/off ratio of 3.3×10^6, which is among the highest mobilities shown by polycrystalline thin films of chrysene derivatives.[19,20]

Results and discussion

Synthetic procedures

The synthetic routes of chrysene derivatives Ph-CHR and C12-Ph-CHR are shown in Scheme 1. The target organic semiconductor materials can be easily prepared through four simple procedures. First, the compound (*E*/*Z*)-1-[2-(3-bromophenyl)ethenyl]-naphthalene (**3**) was easily synthesized on a large scale from commercially available reagents by the Wittig reaction. In particular, the key intermediate compound 2-bromochrysene (**4**) was synthesized by a photochemical reaction using *cis*/*trans* isomer mixture 1-[2-(3-bromophenyl)ethenyl]naphthalene as a precursor with 92% yield. Ph-CHR and C12-Ph-CHR were synthesized by the Suzuki coupling reaction between **5a** or **5b** and 2-bromochrysene with high yield and pure compounds were obtained by sublimation. The chemical structures were characterized by HRMS and NMR.

Photochemical and thermal properties

In order to obtain the HOMO and LUMO energy levels and study the air stability of the materials, Ph-CHR and C12-Ph-CHR,

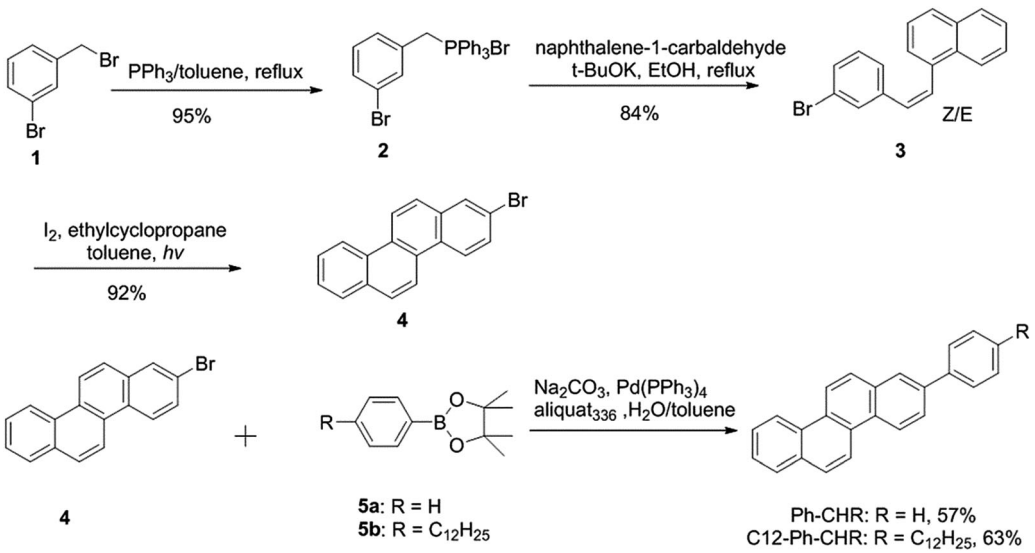

Scheme 1 Synthetic approach for Ph-CHR and C12-Ph-CHR.

 This journal is © The Royal Society of Chemistry 2017

Published on 01 December 2017. Downloaded by University Town Library of Shenzhen on 02/02/2018 01:34:05.

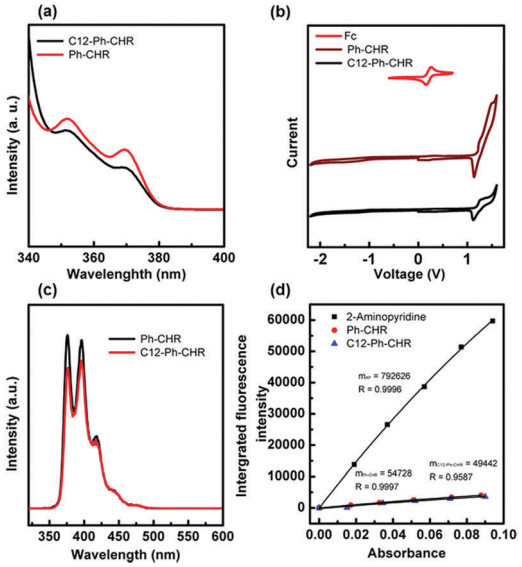

Fig. 3 UV-vis spectra (a), cyclic voltammogram (b), fluorescence spectra (c) and quantum yield (d) of compounds Ph-CHR and C12-Ph-CHR in dichloromethane.

UV-vis spectra and cyclic voltammograms (CVs) of their dichloromethane solutions were tested in nitrogen. Fig. 3a shows the UV-vis spectra of the materials Ph-CHR and C12-Ph-CHR. Our experimental results reveal that these two materials display similar absorption characteristics. The maximum absorption edges of Ph-CHR and C12-Ph-CHR are 380 and 379 nm, indicating that their energy gaps are 3.26 and 3.27 eV, respectively. All the peaks of their fluorescence spectra range from ~350 nm to ~450 nm, showing blue emission (Fig. 3c). The fluorescence quantum yield (Φ) of the materials Ph-CHR and C12-Ph-CHR was measured using 2-amino pyridine as a reference (Fig. 3d).[19] For the estimation of Φ, a 0.1 M H_2SO_4 solution of 2-amino pyridine and dichloromethane was used to prepare solutions of Ph-CHR and C12-Ph-CHR with an optical density of less than 1. From these solutions the fluorescence spectra were taken and by integration, the fluorescence quantum yields of 15% and 20% were estimated for Ph-CHR and C12-Ph-CHR, respectively.

CV tests were carried out to measure the HOMO energy levels of the materials Ph-CHR and C12-Ph-CHR under a standard three-electrode cell electrochemical workstation (Fig. 3b). The energy levels were estimated using −4.8 eV as the HOMO level for the standard ferrocene/ferrocenium (Fc/Fc^+) redox system with a dichloromethane solution containing 0.1 M $TBAPF_6$.[20,21] Both Ph-CHR and C12-Ph-CHR exhibit low-lying HOMO levels, estimated to be −5.79 and −5.78 eV, respectively, which are lower than that of BTBT derivatives C_n-Ph-BTBT (n = 0, 6 and 12).[12,14] This indicates that Ph-CHR and C12-Ph-CHR are relatively air stable organic semiconductor materials.[22–24] However, the HOMO levels of those two materials do not match well with the work function of Au (5.1 eV), which hinders the charge injection from organic semiconductors to Au electrodes in OTFTs. The LUMO levels of Ph-CHR and C12-Ph-CHR of −2.53 and −2.51 eV, respectively, can be calculated

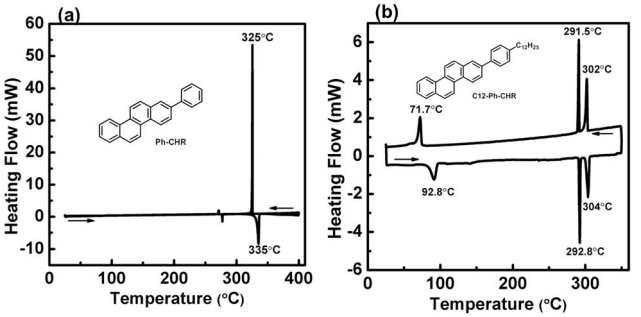

Fig. 4 DSC of Ph-CHR (a) and C12-Ph-CHR (b).

according to the optical band gaps. These values are significantly lower than those of C_n-Ph-BTBT (n = 0, 6 and 12).[12,14]

As shown in Fig. S1 (ESI‡), the materials Ph-CHR and C12-Ph-CHR display good thermal stability with decomposition temperatures of 320 and 340 °C, respectively, as measured by thermogravimetric analysis (TGA). No phase transition is found for Ph-CHR in differential scanning calorimetry (DSC) scans before it began to decompose. In the cooling process, the DSC curve of C12-Ph-CHR shows three phase transitions: an isotropic-liquid crystal (LC1) transition at 302.0 °C, a LC1–LC2 transition at 291.5 °C and a LC2 – crystal transition at 71.7 °C (Fig. 4).

OTFT devices with vapor-deposited thin films

In order to investigate the semiconductor performance of the non-liquid crystalline material Ph-CHR and the liquid crystalline material C12-Ph-CHR, OTFT devices with a bottom-gate/top-contact structure were fabricated by vacuum deposition on OTS(8)-treated Si/SiO_2 substrates and were characterized under ambient conditions. The thickness of the organic semiconductor thin films was about 50 nm. For both Ph-CHR and C12-Ph-CHR, various substrate temperatures (T_{sub}) were selected in order to obtain the best device performance. Table 1 summarizes the OTFT performance including the carrier mobility, on/off current ratio (I_{on}/I_{off}), threshold voltage (V_{th}) and subthreshold swing (S) for each device. Representative output characteristics (I_d–V_d) and transfer characteristics (I_d–V_g) of the OTFTs under various conditions are shown in Fig. 5.

All of the devices exhibit typical p-channel field-effect characteristics under ambient conditions. The average carrier mobility based on eight devices for Ph-CHR is 0.084 $cm^2\ V^{-1}\ s^{-1}$, which is higher than that for Ph-BTBT-based OTFTs, and substrate temperature has no obvious effect on the OTFT device performance. The C12-Ph-CHR-based OTFTs show better device performance than Ph-CHR-based OTFTs under the same conditions. The OTFTs based on C12-Ph-CHR and fabricated at T_{sub} = 25 °C display a mobility as high as 0.86 $cm^2\ V^{-1}\ s^{-1}$ and an average mobility of 0.56 ± 0.17 $cm^2\ V^{-1}\ s^{-1}$. It is worth noting that the mobility of OTFTs fabricated in this condition varied in a relatively broader range, which indicates that the thin films are not very uniform. It is interesting to note that the liquid crystal material C12-Ph-CHR tends to obtain higher mobility in the devices fabricated at the higher substrate temperatures. The OTFTs fabricated at T_{sub} = 60 °C show a

Published on 01 December 2017. Downloaded by University Library of Shenzhen on 02/02/2018 01:34:05.

Table 1 The OTFT performances of Ph-CHR and C12-Ph-CHR

Compound	T_{sub}[a] (°C)	μ_{sat}[b] [cm^2 V^{-1} s^{-1}]	I_{on}/I_{off}	V_{th} (V)	S
Ph-CHR	25	0.084 ± 0.042 (0.15)	(7.7 ± 4.4) × 10^3	−82.7 ± 0.2	6.9 ± 0.5
	60	0.014 ± 0.008 (0.020)	(8.4 ± 5.1) × 10^2	−84.3 ± 0.2	5.7 ± 0.1
C12-Ph-CHR	25	0.56 ± 0.17 (0.86)	(3.0 ± 1.5) × 10^5	−47.6 ± 1.0	8.1 ± 0.4
	25 (doping)[c]	0.57 ± 0.06 (0.65)	(2.4 ± 0.1) × 10^5	−39.9 ± 1.0	6.9 ± 0.5
	60	2.03 ± 0.51 (2.71)	(4.0 ± 2.3) × 10^5	−48.9 ± 0.4	7.0 ± 0.3
	90	2.30 ± 0.35 (3.07)	(2.5 ± 0.6) × 10^5	−46.5 ± 0.4	10.1 ± 0.3
	120	1.01 ± 0.32 (1.44)	(2.2 ± 0.9) × 10^5	−51.5 ± 0.5	6.6 ± 0.6

Note: [a] Substrate temperature. [b] All the data were reported as the average value from more than 5 devices. The values in parentheses represent the maximum mobility. [c] The OTFT devices were doped with F4-TCNQ.

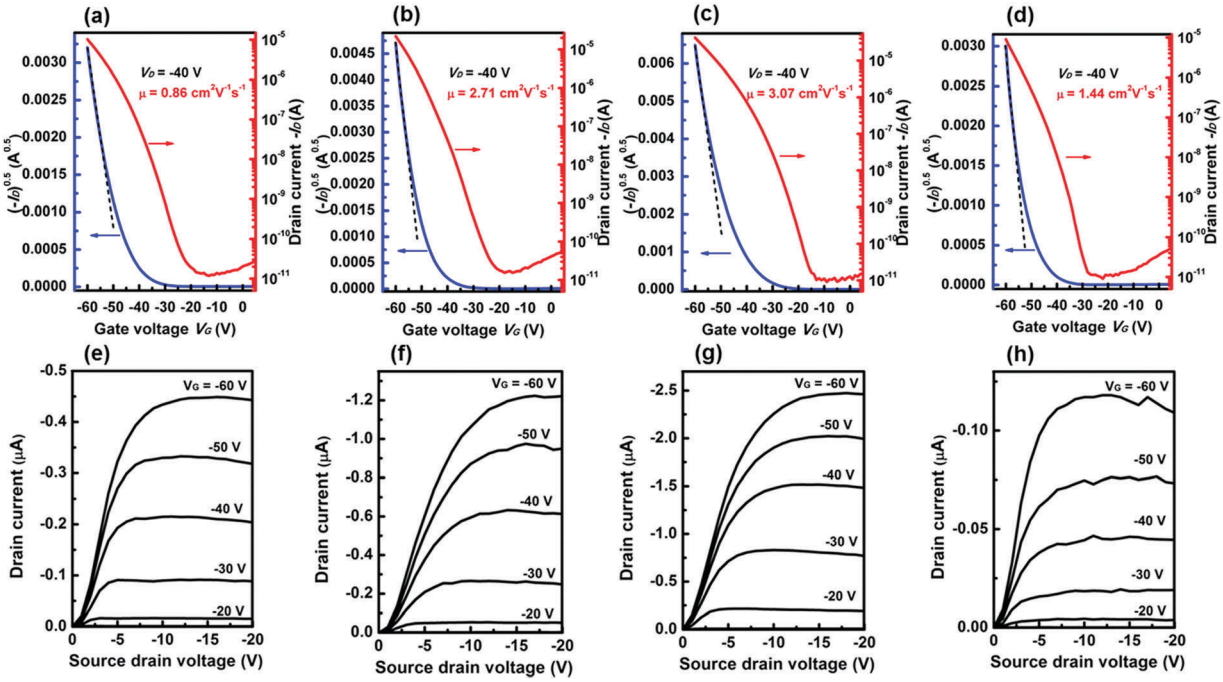

Fig. 5 Transfer and output curves of OTFTs of C12-Ph-CHR films grown on OTS-treated substrates at T_{sub} = 25 °C (a and e), 60 °C (b and f), 90 °C (c and g), and 120 °C (d and h). (a–d) I_d–V_g characteristics curves; (e–h), I_d–V_d characteristics curves.

higher on-current and a higher mobility of 2.03 ± 0.51 cm^2 V^{-1} s^{-1}. This value is four times higher than the former. As shown in Fig. 5c, the devices fabricated at T_{sub} = 90 °C show relatively higher carrier mobility. OTFTs based on C12-Ph-CHR exhibit an average mobility of 2.30 ± 0.35 cm^2 V^{-1} s^{-1} and an on/off current ratio over 10^5 as measured for five devices. In particular, the highest mobility of up to 3.07 cm^2 V^{-1} s^{-1} was achieved for the C12-Ph-CHR-based OTFTs in the saturation regime, which is higher than that of the mobility of the parent chrysene-based devices and comparable with the highest mobility so far reported for OTFTs based on polycrystalline thin films of chrysene derivatives as the active hole transporting layers. This result indicates that the polycrystalline films of C12-Ph-CHR fabricated at T_{sub} = 90 °C are less defective. However, the OTFT performance decreases with the further increase in substrate temperature. We attribute low mobility to the discontinuity of the film caused by cracks produced at high substrate temperature (see the following discussion on the film morphology). Unfortunately, all the devices show high threshold voltages. This may be due to the mismatch of the HOMO levels of Ph-CHR and C12-Ph-CHR (∼−5.78 eV) with the work function of gold (5.1 eV), and hampered charge injection caused by the charge trap states. Doping of the semiconductor materials with an additional electron acceptor, such as molybdenum oxide (MoO_x) and 2,3,5,6-tetrafluoro-7,7,8,8-tetracyanoquinodimethane (F4-TCNQ), could decrease the V_{th} of the OTFT devices.[25–29] In the present study, the OTFTs based on as-deposited C12-Ph-CHR were doped with F4-TCNQ.[28] The experimental results indicate that the F4-TCNQ treatment can decrease the threshold voltages and contact resistance without reducing the charge mobility of the OTFTs based on as-deposited C12-Ph-CHR (Table 1 and Fig. 6).

Morphology of vapor-deposited thin films

To study the relationship between thin film morphology and OTFT device performance, we further study the polycrystalline thin films based on Ph-CHR and C12-Ph-CHR fabricated at various substrate temperatures by atomic force microscopy

 This journal is © The Royal Society of Chemistry 2017

Published on 01 December 2017. Downloaded by University Library of Shenzhen on 02/02/2018 01:34:05.

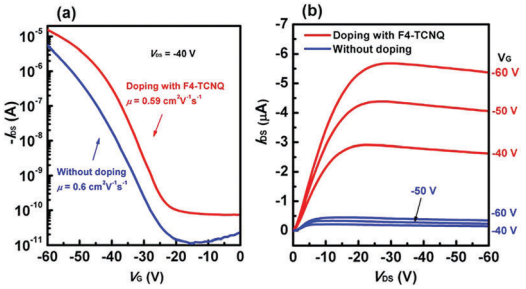

Fig. 6 C12-Ph-CHR-based OTFT characteristics: (a) transfer curve (I_d–V_g characteristics) and (b) output curve (I_d–V_d characteristics) of the as-deposited device (without doping) and the devices doped with F4-TCNQ.

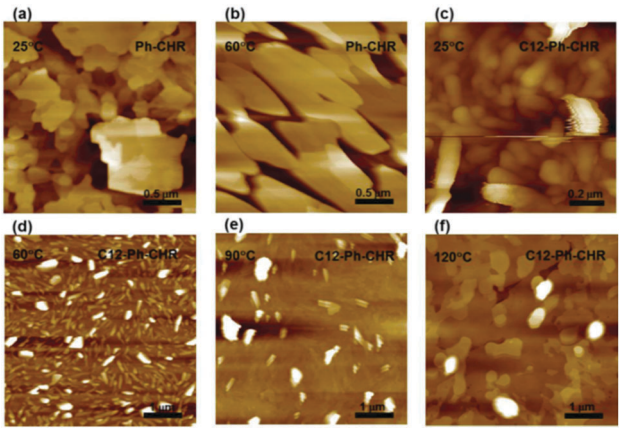

Fig. 7 AFM height images of thin-films of Ph-CHR as-deposited (a) and fabricated at T_{sub} = 60 °C (b), and the films of C12-Ph-CHR deposited at different substrate temperatures: (c) as-deposited, (d) 60 °C, (e) 90 °C, and (f) 120 °C, respectively.

(AFM) and thin film X-ray diffraction (XRD). Fig. 7 shows the AFM images of the thin-films of Ph-CHR and C12-Ph-CHR on the OTS(8)-treated Si/SiO_2 substrates deposited at various substrate temperatures. The substrate temperature significantly influences the crystalline domain sizes of the thin-films based on Ph-CHR, as shown in Fig. 7a and b. The surface of the films develops larger domains with the increase in substrate temperature. According to the literature, the larger domain size contributes to the improvement in carrier mobility.[30] However, in the thin-films of Ph-CHR deposited at T_{sub} = 60 °C, non-continuous crystallites are observed, which cause weaker OTFT device performance than that of OTFTs deposited at T_{sub} = 25 °C. For C12-Ph-CHR, the uniformity of the thin-films on the substrate is also tremendously influenced by the substrate temperature; the thin film morphology transforms from a relatively rough surface at room temperature (Fig. 7c) to progressively more uniform with increase in the substrate temperature (Fig. 7d and e). This result of thin-film morphology is consistent with the OTFT device performance. The thin-films have a smoother surface, and the OTFTs exhibit higher mobility. The films based on C12-Ph-CHR as deposited at T_{sub} = 90 °C have the lowest RMS roughness with a corresponding highest mobility of 3.07 $cm^2 V^{-1} s^{-1}$. At the higher substrate temperature

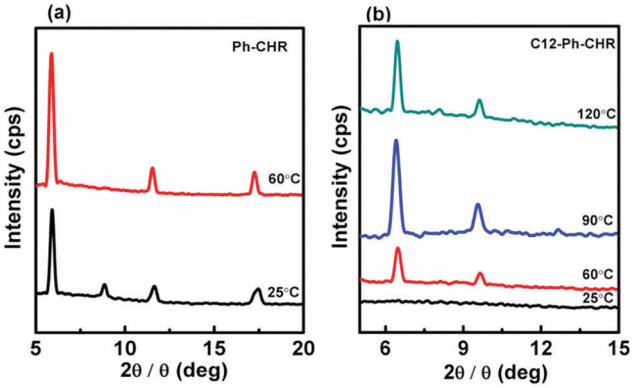

Fig. 8 Thin-film XRD pattern of Ph-CHR (a) and C12-Ph-CHR (b) as deposited at various substrate temperatures.

(T_{sub} = 120 °C), a large number of cracks are observed in the films owing to the strong crystallization of the C12-Ph-CHR. The mobility of OTFTs fabricated at T_{sub} = 120 °C decreases to 1.01 ± 0.32 $cm^2 V^{-1} s^{-1}$ (Fig. 7f).

Fig. 8 shows the thin-film XRD patterns of Ph-CHR and C12-Ph-CHR fabricated under various conditions. The thin-film XRD patterns of both Ph-CHR and C12-Ph-CHR display higher order reflections with the increase in substrate temperature, indicating a higher order in thin films deposited at higher substrate temperatures. The thin-film XRD patterns of C12-Ph-CHR present the highest order reflection in the thin-films deposited at T_{sub} = 90 °C. When T_{sub} increased to 120 °C, the intensity of the peaks weakens because of the cracks in the thin film. All the results of thin film morphology agree with the OTFT device performance.

Experimental

General

All chemicals and solvents used were analytical reagents. The synthetic route of chrysene derivatives Ph-CHR and C12-Ph-CHR is presented in Scheme 1. (*E*/*Z*)-1-[2-(3-Bromophenyl)-ethenyl]naphthalene (**3**) and 2-(4-dodecylphenyl)-4,4,5,5-tetramethyl-1,3,2-dioxaborolane (**5b**) were prepared according to the reported methods.[12,31] The chemical structures were confirmed by ^{1}H NMR and H RMS. Thermo-gravimetric analysis (TGA) was measured on a TA Instruments TA2950 TGA system at a heating rate of 15 °C min^{-1} and a nitrogen flow rate of 60 cm^3 min^{-1}. Differential scanning calorimetry (DSC) was carried out on a TA Instruments DSC Q1000 at a heating or cooling rate of 10 °C min^{-1} under a nitrogen flow. Thin-film morphology was studied in atomic force microscopy (AFM) on a SPA400HV instrument with a SPI 3800 controller (Seiko Instruments). XRD patterns were recorded using a Bruker D8 advance X-ray diffractometer with a Cu Kα source (λ = 1.541 Å). The characteristics of the OTFT devices were measured at room temperature under dark ambient conditions using a Keithly 4200 semiconductor parameter analyzer.

Synthesis

2-Bromochrysene (4). (*E*/*Z*)-1-[2-(3-Bromophenyl)ethenyl] naphthalene (3, 6.18 g, 20 mmol) and iodine (6.1 g, 24 mmol)

Published on 01 December 2017. Downloaded by University Town Library of Shenzhen on 02/02/2018 01:34:05.

were dissolved in toluene (1 L) and placed in a photochemical vessel. The mixture solution was degassed by purging with nitrogen for 30 min. Then 2-ethyloxirane (14.4 g, 0.2 mol) was added and the resultant solution was irradiated with a halogen lamp (600 W, ~450 nm). After the reaction was completed, the mixture was concentrated. The pure product was obtained by recrystallization from petroleum ether. ^{1}H NMR (300 MHz, $CDCl_3$) δ 8.82–8.70 (m, 2H), 8.64 (dd, J = 9.0, 3.3 Hz, 2H), 8.14 (d, J = 2.1 Hz, 1H), 8.07–7.97 (m, 2H), 7.91 (d, J = 9.1 Hz, 1H), 7.77 (dt, J = 5.3, 2.7 Hz, 1H), 7.74–7.61 (m, 2H); ^{13}C NMR (75 MHz, $CDCl_3$) δ 133.43, 132.39, 132.15, 131.67, 130.53, 129.74, 129.09, 128.57, 128.20, 127.81, 126.88, 126.59, 126.13, 124.97, 123.06, 122.43, 120.80, 120.37.[32]

2-Phenyl chrysene (Ph-CHR) and 2-(4-dodecylphenyl) chrysene (C12-Ph-CHR). 2-Bromochrysene **4** (10 mmol), **5a** or **5b** (15 mmol), 15 mmol (2 mol L^{-1}) K_2CO_3 and methyl trioctyl ammonium chloride (15 mmol) were added to a Schleck flask. The mixture solution was degassed by purging with N_2 for 20 min. Then $Pd(PPh_3)_4$ was added and the reaction mixture was stirred for two days at 110 °C. Then the reaction mixture was poured into methanol after cooling down to room temperature. The precipitate was filtered off, and washed with water and methanol. The crude products were further purified by sublimation to obtain white powder Ph-CHR and C12-Ph-CHR. Ph-CHR: ^{1}H NMR (300 MHz, $CDCl_3$) δ 8.98–8.67 (m, 4H), 8.22 (d, J = 1.8 Hz, 1H), 8.12–7.93 (m, 4H), 7.90–7.78 (m, 2H), 7.77–7.57 (m, 2H), 7.54 (t, J = 7.5 Hz, 2H), 7.42 (t, J = 7.4 Hz, 1H). HRMS (+ESI) m/z calcd for $C_{24}H_{17}$ $(M + H)^+$ 305.1330, found 305.1319; C12-Ph-CHR: ^{1}H NMR (400 MHz, $CDCl_3$) δ 8.91–8.73 (m, 5H), 8.22 (d, J = 1.7 Hz, 1H), 8.12–7.96 (m, 5H), 7.74 (dd, J = 7.4, 4.0 Hz, 3H), 7.67 (t, J = 7.4 Hz, 1H), 7.36 (d, J = 8.0 Hz, 2H), 2.76–2.62 (m, 2H), 1.77–1.62 (m, 3H), 1.34 (d, J = 35.9 Hz, 24H), 0.91 (t, J = 6.8 Hz, 4H). HRMS (+ESI) m/z calcd for $C_{36}H_{41}$ $(M + H)^+$ 473.3208, found 473.3195.

Fabrication and characterization of OTFT devices. OTFTs were fabricated in a top-contact, bottom-gate configuration on Si/SiO_2 substrates at various substrate temperatures. The substrates were cleaned with deionized water, acetone and isopropanol, and dried with nitrogen before irradiating them with UV for 10 min. Then the substrates were treated with OTS (8) according to the reported procedure.[12] The thin-film (~50 nm thick) of Ph-CHR or C12-Ph-CHR as the active layer was vacuum-deposited on the Si/SiO_2 substrates kept at various temperatures at a rate of 1.0–2.0 Å s^{-1} under high vacuum (~2.0×10^{-4} Pa) conditions. The gold films (~50 nm) as drain and source electrodes were deposited using a shadow mask. For the fabrication of doped devices, the as-deposited films were dipped in 5 mmol L^{-1} solution of F4-TCNQ in CH_3CN and dried with nitrogen, before the deposition of the electrodes. For a typical device, the drain–source channel width (W)/length (L) are 380 μm/38 μm, 580 μm/58 μm, 780 μm/78 μm, and 980 μm/98 μm, respectively. The field-effect mobility (μ_{FTF}) was estimated from the saturation regime (V_d = −40 V) of the I_d by employing the following formula:

$$I_d = (W/2L)\mu_{TFT}C_i(V_g - V_{th})^2$$

where C_i indicates the capacitance of the SiO_2 insulator, and V_g and V_{th} represent the gate and threshold voltages, respectively. The on/off current ratio (I_{on}/I_{off}) was determined from the current I_d at V_g = −60 V and V_g = 0 V.

Conclusions

In the present work, we designed and efficiently synthesized a non-liquid crystalline material of Ph-CHR and a novel liquid crystalline material of C12-Ph-CHR with thermal stability and durability. Being isoelectronic, [1]benzothieno[3,2-*b*]benzothiophene and chrysene possess similar energy levels. The synthesis of chrysene derivatives is very simple, by introducing a photochemical reaction, compared with that of the [1]benzothieno[3,2-*b*]benzothiophene derivatives. The average carrier mobility of the OTFTs based on Ph-CHR is 0.084 $cm^2 V^{-1} s^{-1}$, which is higher than that of OTFTs based on the BTBT derivative Ph-BTBT. It is intriguing that the performance of the OTFTs based on C12-Ph-CHR is dramatically improved with the increase in substrate temperature. The OTFTs based on C12-Ph-CHR fabricated at T_{sub} = 90 °C achieved the maximum mobility of 3.07 $cm^2 V^{-1} s^{-1}$, which is, to the best of our knowledge, one of the highest values for thin film transistors based on chrysene derivatives. Based on these results, we conclude that chrysene derivative C12-Ph-CHR can be a potential candidate for practical application in future organic electronics.

Conflicts of interest

There are no conflicts to declare.

Acknowledgements

This work was financially supported by National Natural Science Foundation of China (Grant No. 51603003), Shenzhen Science and Technology Research Grant (JCYJ20170412151139619, JCYJ20160331095335232, JCYJ20160331095335232), the Shenzhen Peacock Program (KQTD2014062714543296), Guangdong Key Research Project (No. 2014B090914003, 2015B090914002), National Basic Research Program of China (973 Program, No. 2015CB856500), China Postdoctoral Science Foundation (2015M570892), and Natural Science Foundation of Guangdong Province (2014A030313800).

Notes and references

1 C. D. Dimitrakopoulos and P. R. Malenfant, *Adv. Mater.*, 2002, **14**, 99–117.
2 G. Gelinck, P. Heremans, K. Nomoto and T. D. Anthopoulos, *Adv. Mater.*, 2010, **22**, 3778–3798.
3 W.-L. Liau, T.-H. Lee, J.-T. Chen and C.-S. Hsu, *J. Mater. Chem. C*, 2016, **4**, 2284–2288.
4 H. Iino, T. Usui and J. Hanna, *Nat. Commun.*, 2015, **6**, 6828.
5 J. Seo, S. Park, S. Nam, H. Kim and Y. Kim, *Sci. Rep.*, 2013, **3**, 2452.

 This journal is © The Royal Society of Chemistry 2017

Published on 01 December 2017. Downloaded by University Town Library of Shenzhen on 02/02/2018 01:34:05.

6 A. Kim, K. S. Jang, J. Kim, J. C. Won, M. H. Yi, H. Kim, D. K. Yoon, T. J. Shin, M. H. Lee, J. W. Ka and Y. H. Kim, *Adv. Mater.*, 2013, **25**, 6219–6225.
7 H. Iino, T. Kobori and J.-i. Hanna, *J. Non-Cryst. Solids*, 2012, **358**, 2516–2519.
8 H. Iino and J.-i. Hanna, *J. Appl. Phys.*, 2011, **109**, 074505.
9 H. Iino and J. Hanna, *Adv. Mater.*, 2011, **23**, 1748–1751.
10 W. Pisula, M. Zorn, J. Y. Chang, K. Müllen and R. Zentel, *Macromol. Rapid Commun.*, 2009, **30**, 1179–1202.
11 A. J. van Breemen, P. T. Herwig, C. H. T. Chlon, J. Sweelssen, H. F. M. Schoo, S. Setayesh, W. M. Hardeman, C. A. Martin, D. M. de Leeuw, J. J. P. Valeton, C. W. M. Bastiaansen, D. J. Broer, A. R. Popa-Merticaru and S. C. J. Meskers, *J. Am. Chem. Soc.*, 2006, **128**, 2336–2345.
12 Y. He, M. Sezen, D. Zhang, A. Li, L. Yan, H. Yu, C. He, O. Goto, Y.-L. Loo and H. Meng, *Adv. Electron. Mater.*, 2016, **2**, 1600179.
13 C. He, Y. He, A. Li, D. Zhang and H. Meng, *Appl. Phys. Lett.*, 2016, **109**, 143302.
14 Y. He, W. Xu, I. Murtaza, D. Zhang, C. He, Y. Zhu and H. Meng, *RSC Adv.*, 2016, **6**, 95149–95155.
15 G. A. Petersson, A. Bennett, T. G. Tensfeldt, M. A. Al-Laham, W. A. Shirley and J. Mantzaris, *J. Chem. Phys.*, 1988, **89**, 2193.
16 G. A. Petersson and M. A. Al-Laham, *J. Chem. Phys.*, 1991, **94**, 6081.
17 A. D. Becke, *J. Chem. Phys.*, 1993, **98**, 5648–5652.
18 M. Abe, T. Mori, I. Osaka, K. Sugimoto and K. Takimiya, *Chem. Mater.*, 2015, **27**, 5049–5057.
19 R. Rusakowicz and A. C. Testa, *J. Chem. Phys.*, 1968, **72**, 2680–2681.
20 Y. Liang, Y. Wu, D. Feng, S.-T. Tsai, H.-J. Son, G. Li and L. Yu, *J. Am. Chem. Soc.*, 2009, **131**, 56–57.
21 C. M. Cardona, W. Li, A. E. Kaifer, D. Stockdale and G. C. Bazan, *Adv. Mater.*, 2011, **23**, 2367–2371.
22 D. de Leeuw, M. Simenon, A. Brown and R. Einerhand, *Synth. Met.*, 1997, **87**, 53–59.
23 W. Wu, Y. Liu and D. Zhu, *Chem. Soc. Rev.*, 2010, **39**, 1489–1502.
24 C. Wang, H. Dong, W. Hu, Y. Liu and D. Zhu, *Chem. Rev.*, 2012, **112**, 2208–2267.
25 D. Kumaki, Y. Fujisaki and S. Tokito, *Org. Electron.*, 2013, **14**, 475–478.
26 P. Jeon, K. Han, H. Lee, H. S. Kim, K. Jeong, K. Cho, S. W. Cho and Y. Yi, *Synth. Met.*, 2009, **159**, 2502–2505.
27 Y. Zhang, B. de Boer and P. W. M. Blom, *Adv. Funct. Mater.*, 2009, **19**, 1901–1905.
28 J. Soeda, Y. Hirose, M. Yamagishi, A. Nakao, T. Uemura, K. Nakayama, M. Uno, Y. Nakazawa, K. Takimiya and J. Takeya, *Adv. Mater.*, 2011, **23**, 3309–3314.
29 C.-W. Chu, S.-H. Li, C.-W. Chen, V. Shrotriya and Y. Yang, *Appl. Phys. Lett.*, 2005, **87**, 193508.
30 R. L. Headrick, S. Wo, F. Sansoz and J. E. Anthony, *Appl. Phys. Lett.*, 2008, **92**, 063302.
31 S. Ito, M. Wehmeier, J. D. Brand, C. Kübel, R. Epsch, J. P. Rabe and K. Müllen, *Chem. – Eur. J.*, 2000, **6**, 4327–4342.
32 A. Mueller and K. Y. Amsharov, *Eur. J. Org. Chem.*, 2012, 6155–6164.